Optics & Laser Technology 88 (2017) 263–274

Contents lists available at ScienceDirect

Optics & Laser Technology

journal homepage: www.elsevier.com/locate/optlastec

Full length article

Tunable CO_2 laser system with subnanosecond-pulse-train output

W.D. Kimura

STI Optronics, Inc., 2647 – 151st Place NE, Redmond, WA 98052 USA

ARTICLE INFO

Keywords:
CO_2 laser
Optical free induction decay
Subnanosecond

ABSTRACT

A CO_2 laser system has been demonstrated that generates a train of subnanosecond pulses tunable over the *P* and *R* branches of the CO_2 laser spectrum at 9–11 μm. It utilizes optical free induction decay to generate a single ~100-ps laser pulse from a tunable transverse-excited-atmospheric CO_2 laser. This laser pulse is injection-seeded into a high-pressure CO_2 oscillator whose output consists of a train of amplified ~100-ps pulses with maximum pulse energy of 30 mJ, corresponding to a peak power of 300 MW. The ~100-ps, tunable, infrared laser pulses are needed for a new technique to remotely detect atmospheric gaseous molecules, which relies on the train of CO_2 laser pulses selectively exciting the target molecules whose presence is then revealed using a separate terahertz probe beam.

1. Introduction

There is keen interest in developing ultrashort-pulse carbon dioxide (CO_2) lasers for applications such as laser-driven electron [1] and proton [2] acceleration, and Compton scattering *x*-ray sources [3]. Indeed, pulse lengths as short as a few picoseconds have been demonstrated [4,5]. However, as explained below, certain applications require of order 100-ps pulse lengths that are tunable over all the CO_2 laser lines.

Remote detection of gaseous chemical agents can be important for military and anti-terrorism applications. While discrete devices are available for sensing these agents, the widespread field deployment of these devices is impractical, especially during military operations. A laser system utilizing differential absorption lidar (DIAL) can be used to remotely detect these agents and is attractive because the laser beam can be swept 360° around the perimeter and from the horizon to the zenith. However, DIAL suffers from a fundamental limitation. It relies on detecting the absorption of the laser light tuned to the resonance of the target molecule. Atmospheric pressure broadening causes the absorption spectrum of the target species to overlap with the spectrum of other gases, thereby interfering with the unambiguous identification of the agents. This greatly diminishes the effectiveness of DIAL for this application.

This problem can be overcome by utilizing a novel double-resonance technique [6] in which a CO_2 laser beam excites the molecules of interest at a remote distance. A separate THz beam is sent to probe these excited molecules and results in emission at specific THz frequencies unique to each molecule. The modulated signal can be detected via background retro-reflection or backscattered light using highly sensitive THz detectors. This technique provides a sensitive method for uniquely identifying the molecules via a 3-D specificity matrix whose parameters consist of the CO_2 laser frequency, the THz probe frequency, and the time-resolved THz signal relaxation characteristics [6].

This double-resonance remote sensing (DRRS) technique establishes a new paradigm where the CO_2 laser beam only excites the molecules of interest rather than relies on resonant absorption. Consequently, atmospheric broadening actually helps the process by making it easier to excite the molecules off-resonance. This innovation can help expand the usage of lidar systems for atmospheric detection of trace gases.

DRRS relies on the rapid molecular collisional relaxation time, which at atmospheric pressure and temperature is of order 100 ps. Therefore, an ultrashort, ~100-ps laser pulse is needed so that this excitation pulse together with the rapid collisional relaxation can modulate the molecular THz emission or absorption on a time scale much faster than the ~1 s temporal atmospheric fluctuations. This is important for separating the molecular signal from signals due to clutter. The laser output wavelength also needs to be tunable over the 9–11 μm region in order to resonantly excite the molecules of interest. A pulse energy ≥10 mJ is needed for sensing at ranges of order 100 m [6]. Higher pulse energy will allow extending the sensing range. A pulse train is also highly desirable because it permits averaging over many pulses, thereby improving the signal-to-noise ratio (SNR). This will help increase the sensing range and enable more rapid scanning of air regions. Ultimately, the laser system must be portable and durable enough for deployment in the field. This implies the need to keep the CO_2 laser system as simple as possible in its design and operation.

E-mail address: wkimura@stioptronics.com.

http://dx.doi.org/10.1016/j.optlastec.2016.09.022
Received 1 June 2016; Received in revised form 22 August 2016; Accepted 14 September 2016

This paper describes a tunable CO_2 laser system that generates a train of pulses with pulse lengths ~100 ps and pulses energies > 10 mJ. This system was designed and constructed to satisfy the needs for DRRS. As explained next, while various methods are possible for generating ultrashort CO_2 laser pulses, what distinguishes this work is its wavelength tunability and production of a train of pulses.

2. Design theory

For the DRRS application, pulsed transverse-excited-atmospheric (TEA) CO_2 lasers are the logical choice due to their high pulse energy, relatively compact design, well-established technology, and commercial availability. However, TEA CO_2 lasers typically have output pulse lengths of order 50–100 ns in a gain-switched spike. Various methods are possible for shortening the pulse length.

Q-switching of CO_2 lasers is possible [7–9]. Although high pulse energies are possible, the pulse lengths cannot be reduced to the subnanosecond level.

Both passive [10] and active mode-locking [11] have been used to generate short pulses. Passive mode-locking is generally more effective than active mode-locking at producing the shortest pulse lengths [12] with durations as short as 150 ps demonstrated [11]. However, passive mode-locking is also more difficult to control, especially if the individual pulses must be temporally synchronized with other pulses, such as with the THz probe for DRRS. A more serious issue is that DRRS requires the ability to readily tune to different wavelengths. Reestablishing mode-locking every time the wavelength is changed would be very difficult to do, especially in a field-deployed system.

Optical semiconductor switching [13], in which the CO_2 laser pulse passes through a semiconductor plate oriented at Brewster's angle to truncate the laser pulse, is an effective means for producing a shorter pulse with a controlled pulse length. A separate, fast-risetime, near-infrared (NIR) laser pulse illuminates the plate and creates free electrons (carriers) on the plate surface. These carriers act to reflect the CO_2 light, thereby truncating the CO_2 laser pulse length. Two plates are typically used to slice the front and rear of the laser pulse [14–16]. The minimum length of the sliced pulse is only limited by the risetime rate or, equivalently, the minimum pulse duration of the NIR laser beam illuminating the semiconductor slab. Sliced pulse lengths as short as 130 fs have been demonstrated [17]. A similar gating technique to slice the CO_2 pulse utilizes optical Kerr switching where a fast NIR laser pulse is used to switch the Kerr cell [18].

One drawback of semiconductor and optical Kerr switching is it requires a separate, ultrashort-pulse NIR laser to illuminate the semiconductor slabs or Kerr cell. This considerably complicates the system, which is highly unattractive for DRRS due to its adverse impact on system size, reliability, and cost.

More recently, chirped-pulse-amplification (CPA) has been applied to produce ultrafast IR seed pulses [5], in which a solid-state laser system featuring an optical parametric amplifier (OPA) is used to generate a ps seed IR pulse that is subsequently amplified by a CO_2 laser amplifier. Commercial solid-state OPO systems are available that are tunable in the IR region [19]; however, the pulse lengths are either in the nanosecond or picosecond ranges. There tends to be a gap in the ~100 ps pulse length range for solid-state lasers due to the inherent characteristics of the methods used to produce the pulses, i.e., Q-switching or mode-locking.

Quantum cascade lasers (QCL) are able to generate tunable radiation over 3–15 μm [20]. However, these are not viable seed sources for CO_2 lasers. The shortest pulse lengths produced by QCLs are typically 10′s ns [21] with pulse energies of order nJ, which is too low for effective injection seeding. Although progress is being made to produce ps pulses from QCLs [22], it is likely the eventual pulse energies will be again too low and, furthermore, the high-frequency output pulse train from these mode-locked lasers may be incompatible with seeding CO_2 laser amplifiers. Typically, a single subnanosecond pulse is needed as the injection seed and the seed should be generated at the same repetition rate as the CO_2 laser amplifier.

We should emphasize that although some of the preceding techniques are able to produce 100-ps laser pulses, they are often not easily tunable over the CO_2 lasing spectrum. For example, the semiconductor plates used during pulse slicing are oriented at Brewster's angle, which means this angle would need to be adjusted at each lasing wavelength due to the change in the index of refraction as a function of wavelength. Furthermore, this angle change would displace the beam, thereby requiring a realignment of the optical system. Thus, while wavelength-tuning of CO_2 lasers is normally very straightforward using an intracavity grating, typical methods for generating ultrashort CO_2 laser pulses are not necessarily compatible with wavelength tuning. As we shall explain next, our approach distinguishes itself by not only generating a train of 100-ps laser pulses, but also being easily tunable over the CO_2 lasing spectrum.

The technique we chose for generating the ~100-ps pulses is based upon a process called optical free induction decay (OFID) [23], in which the 100-ns CO_2 laser pulse is sent through a plasma shutter and then through a hot cell (400–500 °C) filled with CO_2 gas. The plasma shutter truncates the CO_2 laser pulse, but unlike in semiconductor switching, this truncation is not intended to shorten the CO_2 laser pulse. Instead the truncation generates high-frequency sidebands whose light also enters the hot cell. The purpose of the hot cell is to act as a frequency filter, whereby it selectively absorbs light at the fundamental frequency, but allows the sideband light to pass through [24]. The frequency spectrum of the light exiting the hot cell is therefore much broader than the incoming pulse's frequency bandwidth and, hence, corresponds to pulses with much shorter lengths. OFID-generated pulses as short as 30 ps have been demonstrated [25]. By adjusting the pressure in the hot cell, which essentially changes its filtering characteristics, it is possible to obtain output pulse lengths between 30 and 300 ps [26].

Thus, the OFID technique is able to provide ~100 ps CO_2 laser pulse lengths in an essentially passive manner that are easily wavelength tunable. This makes it less complicated than semiconductor/Kerr cell switching and, consequently, a suitable candidate for DRRS.

After exiting the hot cell, the ~100-ps pulse has a typical energy of order 10′s μJ. A CO_2 laser amplifier is needed to amplify the pulse to useful energy levels. CO_2 lasers rely on vibrational-rotational molecular transitions for the laser emissions, which means the gain profile consists of discrete frequencies separated by ~40–55 GHz (~1.3–1.5 cm^{-1}). This allows the laser to generate discretely tunable radiation over 9–11 μm, but the discrete gain profile also complicates the ability to amplify ultrashort laser pulses because the gain bandwidth is not continuous over the wide bandwidth of the ultrashort pulses. Hence, the CO_2 discrete gain spectrum must be broaden out to amplify the ~100 ps pulse. The easiest way to accomplish this is to operate the CO_2 amplifier at high pressure (e.g., ~10 atm) so that pressure broadening (~5 MHz/Torr) causes the gain line spectra to widen and merge with each other [27]. This pressure broadening of the CO_2 gain spectrum is illustrated in Fig. 1, where Fig. 1(a) shows the discrete gain lines at 1 atm and Fig. 1(b) depicts the smearing together of the gain lines at 10 atm.

An alternative method for broadening the CO_2 laser gain spectrum is to use gas mixtures containing different isotopes of CO_2 [28]. The gain lines are slightly shifted for each isotopic molecule. Hence, the gain profile of a mixture of isotopes contains many more gain lines in between the nominal ones. This helps smooth out the gain profile with pressure broadening still used to blend the gain lines together. The advantage of using isotopic gas mixtures is it can require less gas pressure to smooth out the gain profile. The disadvantage of isotopic gas mixtures is their high expense.

Utilizing strong field broadening of the lasing transition is another means for amplifying picosecond IR pulses that can be done at atmospheric pressures [29]. This was demonstrated using 3-ps pulses.

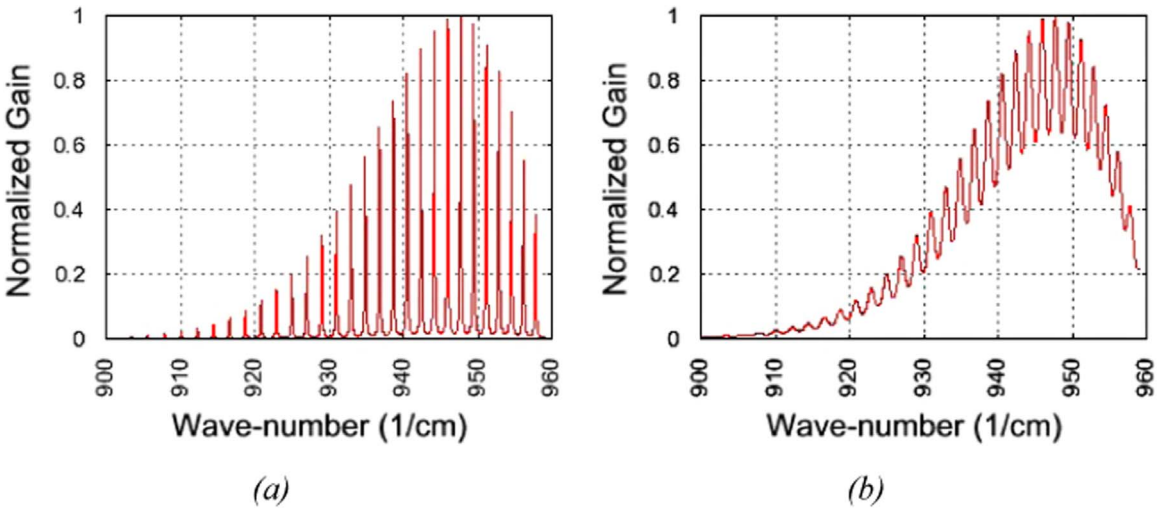

Fig. 1. CO_2 gain spectrum for 10P branch (00°1→10°0) transition at two gas mixture pressures. (a) 1 atm. (b) 10 atm.

It is not clear how well this technique would work for 100 ps pulses especially when the OFID pulse energy is only ~10′s μJ.

As shown in this paper, adequate amplification of the ~100 ps pulse is achievable using a high-pressure amplifier with a non-isotopic CO_2 gas mixture. This high-pressure amplifier is also a commercial product, which helps minimize cost and risks.

Fig. 2 summarizes the basic components of the subnanosecond CO_2 laser system demonstrated in this paper. It consists of a tunable master oscillator (MO) emitting a standard ~100 ns output pulse. The pulse is sent through the plasma shutter and hot cell. Through the OFID process, a ~100 ps pulse exits the hot cell and is sent into a high-pressure CO_2 amplifier whose design details are discussed below. The output of the amplifier consists of a train of amplified micropulses with pulse lengths ~100-ps. As noted later, commercial lasers are used for the MO and high-pressure amplifier.

While non-isotopic, multi-atmospheric CO_2 laser amplifiers have demonstrated the ability to effectively amplify subnanosecond laser pulses [14,24,30], a key design issue is selecting the best amplifier design for amplifying the subnanosecond pulse and producing a pulse train. There are two basic candidate amplifier designs that were considered. The first type is a regenerative amplifier ("regen"). The regen features active optical elements within the amplifier resonator cavity to permit introducing the seed pulse into the cavity, circulating the pulse within the cavity a predetermined number of passes, and then extracting the pulse when the desired amount of amplification has occurred. A schematic of a typical regen layout is shown in Fig. 3. The OFID-generated seed pulse enters the regen from the upper left of the figure. The beam, which is *s*-polarized, reflects off a flat optical plate oriented at Brewster's angle onto the optical axis of the regen and towards Pockels Cell #1 on the left side of the cavity. This Pockels cell rotates the polarization of the light by 90° (*p*-polarized) so that the pulse passes back and forth through the Brewster angle plates and the high-pressure regen discharge chamber. On each pass through the discharge, the pulse gains energy (~2%/cm). By allowing the pulse to make multiple passes through the discharge, it is possible to amplify the pulse up to the saturation fluence limit. However, in practice the maximum amplified pulse energy is limited by the damage threshold of the second Pockels Cell #2 on the right-side of the cavity. This Pockels cell is activated once the circulating pulse has reached the maximum permissible energy level. The cell rotates the polarization of the pulse so that it now reflects off the second Brewster angle plate located near the center of the cavity and exits the regen. Note, the grating at the rear of the regen is important for suppressing amplified spontaneous emission (ASE) by being tuned to the wavelength being amplified, thereby ensuring the regen only amplifies this wavelength.

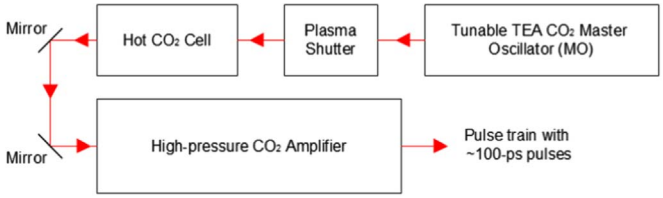

Fig. 2. Schematic layout of ultrashort-pulse CO_2 laser system built and demonstrated in this paper.

It is possible for the regen to produce a train of pulses by simply not extracting all the circulating pulse energy after the multiple passes. Partial extraction of the circulating pulse can be achieved by not fully rotating the polarization of Pockels Cell #2. The portion of the circulating pulse energy that is not extracted is then allowed to multipass once again through the cavity and the partial extraction is repeated over and over again until the circulating pulse lies outside the gain lifetime. We refer to this mode of operation as a partial-extraction regen.

The second candidate for the CO_2 amplifier design is an injection-seeded oscillator whose basic configuration is shown in Fig. 4. The OFID-generated seed pulse is injected through a small injection hole in the rear mirror used to direct light to the tuning grating. The injection hole is intentionally located slightly away from the resonator axis in order to minimize disruption of the beam mode inside the resonator. Despite being slightly off-axis, the seed beam will still effectively provide seed photons within the Frensel core of the resonator when the injection seed is aligned to pass through the center of the output coupler. Once again, the grating serves the important role of suppressing lasing on wavelengths other than the one associated with the injection seed. This is especially important when amplifying the weaker laser lines.

In the injection-seeded oscillator, a portion of the circulating pulse energy passes through the partial reflecting output coupler (OC) after every double-pass through the active medium. Thus, this scheme automatically generates a train of micropulses from a single input seed pulse, where the time separation between the micropulses equals the cavity roundtrip time. The number of micropulses in the train will be determined by the discharge pumping characteristics, which affects how long the gain remains high while the pulse is circulating back and forth within the resonator.

A CO_2 laser model "*co2amp*" developed by Polyanskiy [31] and specifically designed to analyze amplification of ultrashort pulses was used to simulate amplification of a subnanosecond pulse in a partial-extraction regen and injection-seeded oscillator. The model is a 2-D

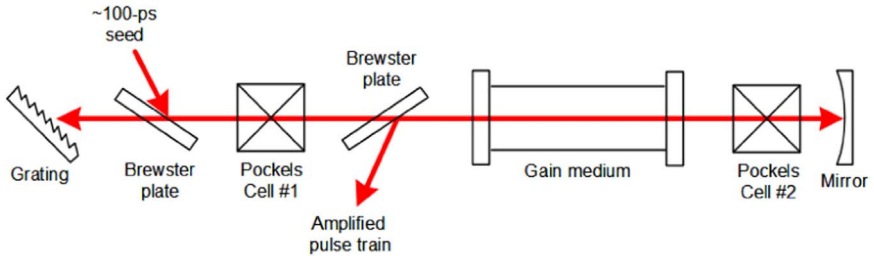

Fig. 3. Schematic diagram of regenerative amplifier.

one that assumes axial symmetry of the beam and the active medium. It simulates propagation through a resonator (including diffraction effects) of a pulse with a given initial energy, duration, intensity distribution, and wavelength. The active medium condition at every point of the calculation is determined by a set of Boltzmann temperatures that represent populations of laser levels and translational/rotational energies. The model has been validated through its extensive usage in simulating the ultrashort-pulse amplification of CO_2 laser pulses being conducted at the Brookhaven National Laboratory Accelerator Test Facility (BNL-ATF) [5].

The model results indicate that both these amplifier configurations can amplify the subnanosecond pulse and generate a pulse train. However, they each have pros and cons. For the partial-extraction regen, its major pro is the ability to amplify even the weakest laser lines by simply allowing the pulse to circulate for more passes before it is extracted. Its cons are its increased complexity compared to the injection-seeded oscillator and optical damage of the Pockels cells, which limits the maximum pulse energy. This limitation cannot be easily circumvented by increasing the beam size within the regen because Pockels cells for IR beams, which are typically made from CdTe, are not readily available in large diameters. They also become prohibitively expensive as the diameter increases due to the increased costs for the larger CdTe crystal and the Pockels cell high-speed driver, which must operate at a correspondingly higher voltage.

The injection-seeded oscillator pros are: 1) A less complex design compared to the regen. The regen has more active components and requires precise timing control of the two Pockels cells, where the timing must be adjusted each time a different laser line is being amplified. 2) Higher maximum pulse energy compared with the regen because it is not limited by Pockels cell damage. And, 3) significantly lower cost due to exclusion of the Pockels cells and their high-voltage drivers. The major con of the injection-seeded oscillator is the inability to amplify very weak laser lines. However, as shown below, this was not a significant drawback. Therefore, for this project, the injection-seeded oscillator was chosen. The basic design parameter values for our injection-seeded oscillator were shown earlier in Fig. 4.

It should be mentioned that the grating used in the injection-seeded oscillator does not limit the oscillator's gain bandwidth, thereby, possibly defeating the gain broadening by operating at high gas pressure. The line narrowing of an intracavity grating goes as $\Delta\nu \propto dL^{1/4}n^{-1/2}\lambda^{-3/4}a^{-3/2}\cos\theta$, where d is the grating spacing, L is the cavity length, n is the number of single cavity transits, λ is the laser wavelength, a is the beam radius on the grating, and θ is the angle of incidence on the grating [32]. The grating has 150 lines/mm. For our specific configuration with a relatively long cavity length (1.25 m), operating the grating at near-normal incidence, a small beam radius on the grating (≈3 mm), and the fact there only two cavity transits per output pulse (n=2) results in $\Delta\nu$ being of order 3600 GHz. Hence, the grating causes no significant bandwidth narrowing.

We should point out that during the pioneering work of Kesselring et al. [24], they demonstrated OFID using a plasma shutter and hot cell to generate 30-ps pulses at a single wavelength (10.6 μm), and amplified the pulse in a double-pass 15-bar CO_2 amplifier. What distinguishes the work in this paper are the following. We generate tunable ~100-ps OFID pulses over the P and R branches of the CO_2 gain spectrum. These ~100-ps pulses are amplified into a train of pulses. Kesselring et al., used a hybrid CO_2 master oscillator operating in a single longitudinal mode, a custom-made 15-bar CO_2 amplifier, and a double-pass 3-m long hot cell. We use a commercial, multi-mode TEA CO_2 oscillator and commercial 8.5-bar CO_2 amplifier both with agile grating tuners. Our hot cell is only 1-m long, but passes the beam six times to yield the same total travel distance in the hot gas as Kesselring et al. We also use internal mirrors inside the hot cell to avoid sending the beam multiple times through the hot cell windows, thereby minimizing optical losses. Thus, our system is considerably less complex, offers more capabilities, and is more compact than Kesselring et al. Details are given in the next section.

3. Materials and methods

3.1. Master oscillator

The Master Oscillator (MO) is the Model WH10 TEA CO_2 laser manufactured by PAR Systems (formerly SDI Lasers). Fig. 5 shows the measured output pulse energies for the WH10 over its emission spectrum when operating on a 2:2:6 CO_2/N_2/He mixture at 1000 mbar. On the 10.6 μm line (10P20) it emits ≈1.7 J. For many of the other lines it produces > 1 J pulses. Even for the relatively weaker lines near the ends of the bands, the pulse energies are > 100 mJ. Its maximum pulse repetition rate is 50 Hz; however, as explained later, the high-pressure, injection-seeded CO_2 oscillator is limited to 3 Hz. Therefore, during nominal operation of the ultrashort-pulse CO_2 laser system, the WH10 operates at 3 Hz. Table 1 lists the other specifications for the MO.

The MO has an optional, computer-controlled agile tuner located at the rear of the laser. It consists of a rotating mirror that directs light at a stationary grating. The control software permits rotating the mirror to select specific laser lines in the P and R branches.

A manually adjustable iris is located inside the MO resonator to reduce the diameter of the output beam, which is nominally

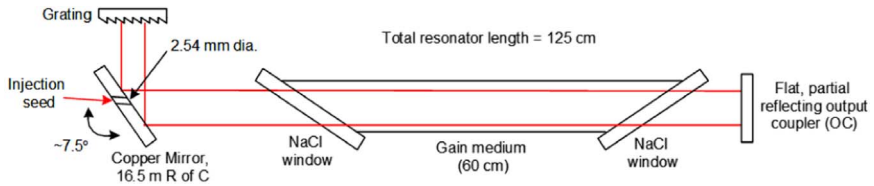

Fig. 4. Schematic diagram of injection-seeded oscillator.

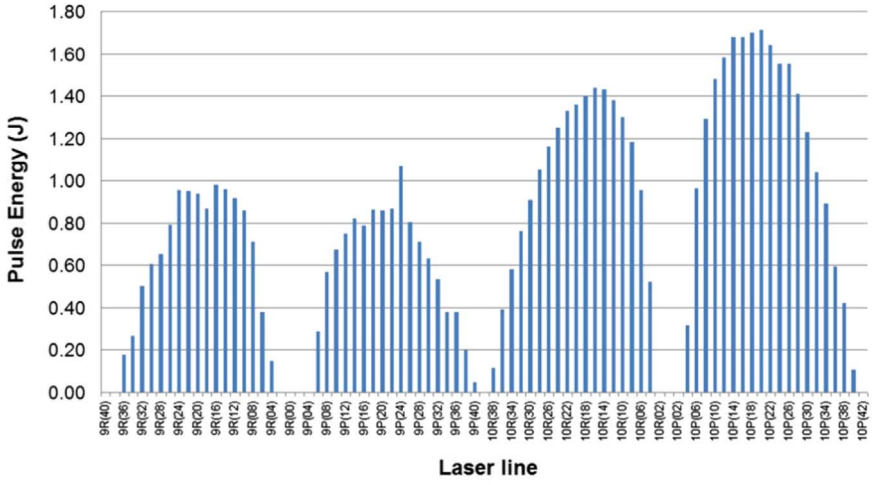

Fig. 5. Measured output laser spectrum for WH10 laser when operating with a 2:2:6 CO_2/N_2/He mixture at nominal operating voltage of 26 kV.

Table 1
WH10 laser specifications.

Average output power (10P20 line, multimode)	5.1 W@3 Hz
Output beam dimensions	18 mm×8 mm
Discharge length	520 mm
Output stability (1–σ)	< 3%
Repetition rate	Nominally 3 Hz (max 50 Hz)
Gas mixture	20% CO_2, 20% N2, 60% He
Gas pressure	950–1000 mbar

1.8 cm×1.8 cm. As explained in Section 3.2, the plasma shutter is limited to input beam sizes of < 1.5 cm diameter. Although the intracavity iris slightly reduces the emitted pulse energy, this did not significantly impact the OFID process.

Fig. 6 shows a typical temporal profile of a pulse produced by the MO (10P20 line) measured using a photovoltaic (PV) detector (time constant ≤1.5 ns) for a 2:2:6 CO_2/N_2/He mixture at 1000 mbar. The gain-switched spike at the beginning of the pulse can be clearly seen and is typically ~100 ns in duration.

The WH10 laser includes a built-in catalytic gas regenerator; hence, its gas lifetime is $> 10^8$ shots. Consequently, since the system operates at a maximum of 3 Hz, the MO gas needs to be rarely replenished. The situation is quite different for the high-pressure, injection-seeded oscillator, which, due to cost limitations, did not have a catalytic gas regenerator and, as explained in Section 3.4, had to have its gas replenished regularly or continuously flow through the device.

3.2. Plasma shutter

The purpose of the plasma shutter is to create a plasma at the peak of the gain-switched spike shown in Fig. 6, thereby, causing an abrupt truncation of the laser pulse and creation of high-frequency components for the OFID process. If the CO_2 laser beam is focused to a small spot size in a gas and if the pulse energy is high enough, then the laser beam will ionize the gas and create a plasma. However, relying on only the laser beam to initiate the plasma formation does not necessarily yield reliable OFID-generated subnanosecond pulses. This is because depending on the type of gas in the plasma shutter, its pressure, and the laser pulse energy, breakdown may occur somewhere besides the peak of the gain-switched spike, such as on the rising edge. This impacts the characteristics of the subnanosecond OFID pulse that is formed by changing the amount of energy distributed in the high-frequency components being generated. Furthermore, on the weak laser lines, the pulse energy is too low to cause breakdown. Earlier researchers who utilized the OFID process were able to operate on a single, strong laser line. For the DRRS application, we must also be able to operate on the weak lines. Hence, we cannot rely solely on laser-induced gas breakdown for the plasma shutter.

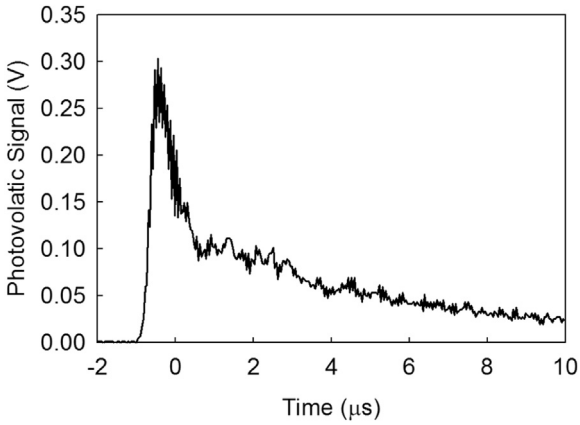

Fig. 6. Typical output pulse temporal profile (10P20 line) from master oscillator obtained using photovoltaic detector.

This issue was addressed by adding a high-voltage spark at the laser focus, which preionizes the gas to help initiate the breakdown process. Fig. 7(a) is a diagram of the interior of the plasma shutter. It consists of a T-shaped vacuum vessel where the CO_2 laser beam from the MO enters and exits through windows in the straight section of the T. Inside this straight section is a pair of meniscus ZnSe lenses (focal length =25.4 mm) that focus the laser beam between the anode and cathode of a high-voltage electrode positioned at the lens focus. The electrode enters the T through the port orthogonal to the straight section. A 35-kV spark is applied across the electrode. The lenses inside the plasma shutter had clear apertures of < 2.3 cm dia. However, the incoming beam from the MO needs to be reduced to 1.5 cm dia. in order to avoid creating a diffraction hot spot (spot of Arago) at the center of the beam, which would damage downstream optics. The shutter is filled with helium gas, which appears to give slightly more reliable performance than using dry nitrogen.

By selecting an appropriate gas pressure and delay time for triggering the 35-kV spark relative to the firing of the MO, gas breakdown could be made to occur near the peak of the gain-switched spike over the tuning range of the MO. Typical helium pressures are 30 Torr; however, on the weakest lines, the pressure needs to be as high as 340 Torr in order to obtain reliable laser-triggered gas breakdown. Examples of the truncated pulse waveforms after passing through the plasma shutter are shown in Fig. 8 for representative lines in the *P* and *R* branches.

Thus, by combining laser-induced gas breakdown with a high-

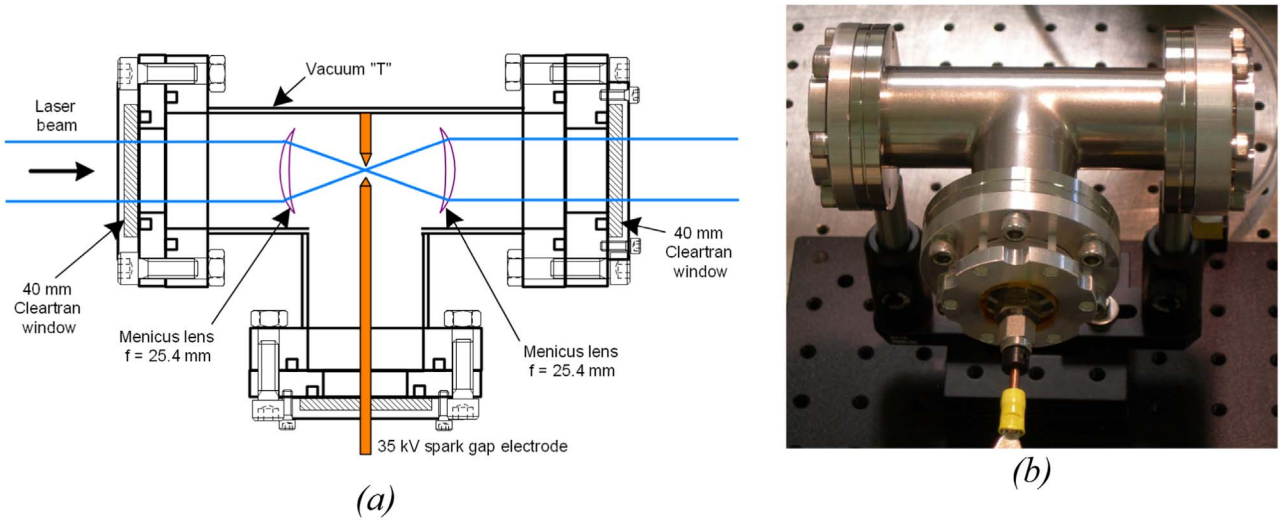

Fig. 7. Plasma shutter. (a) Diagram of interior design. (b) Photograph of plasma shutter.

voltage spark at the laser focus, this plasma shutter design provides controllable and reliable plasma formation over a wide tuning range.

3.3. Hot cell

For their OFID demonstrations, both Kwok et al. [33] and Kesselring et al. [24] used 3-m long CO_2 hot cells where the laser beam doubled passed through the gas yielding a total pathlength of 6 m. The nominal operating temperature of the cell was 400 °C (752°F), which ensured populating the lower (10°0, 02°0) lasing level thermally [33].

In order to make a more compact system for the DRRS application, our hot cell was designed to be 1-m in internal length. The hot cell has adjustable internal mirrors that reflect the CO_2 laser beam six times inside the cell for a total length of 6 m, thereby avoiding optical losses caused by the beam traveling multiple times through windows on the

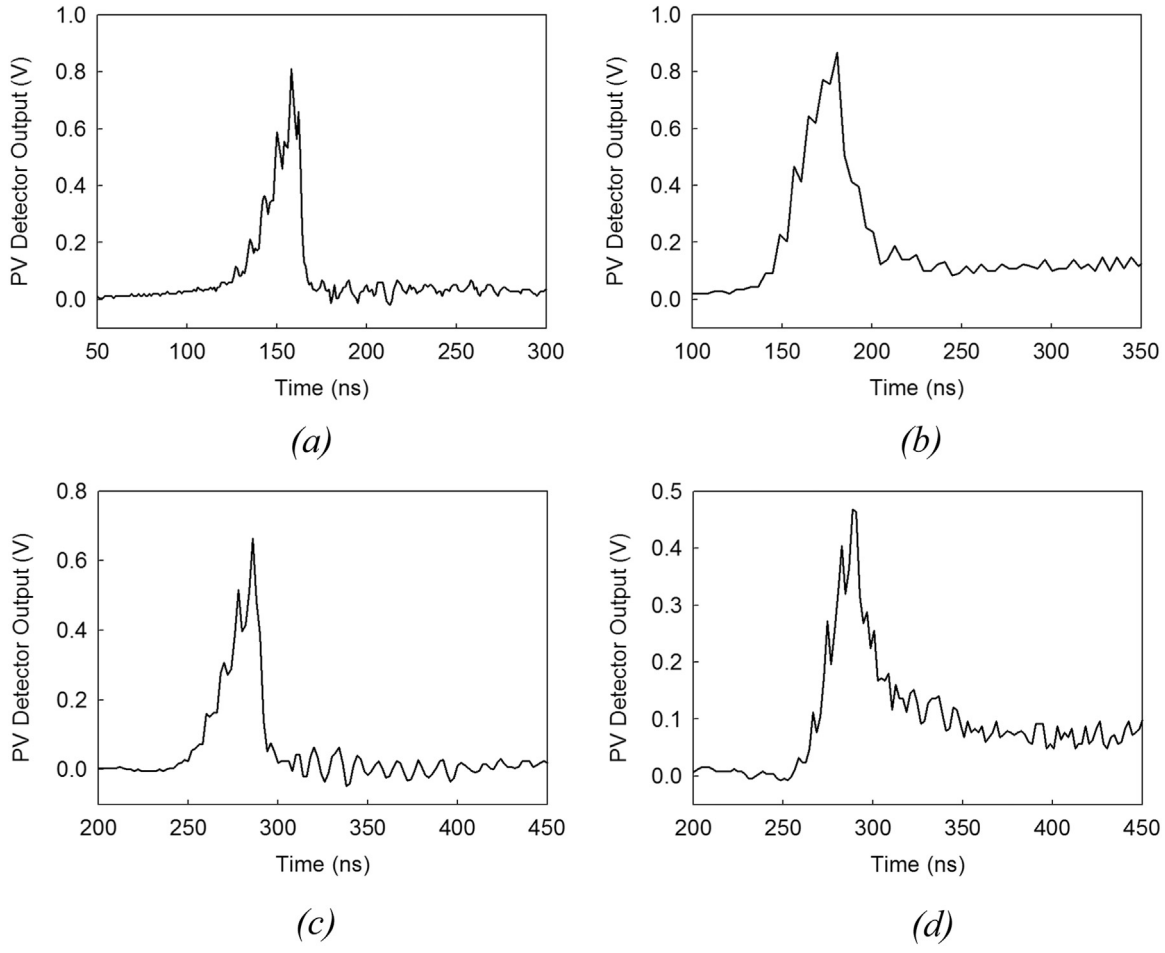

Fig. 8. Examples of truncated pulses exiting the plasma shutter. (a) 9R22 line. (b) 9P20 line. (c) 10R24 line. (d) 10P18 line.

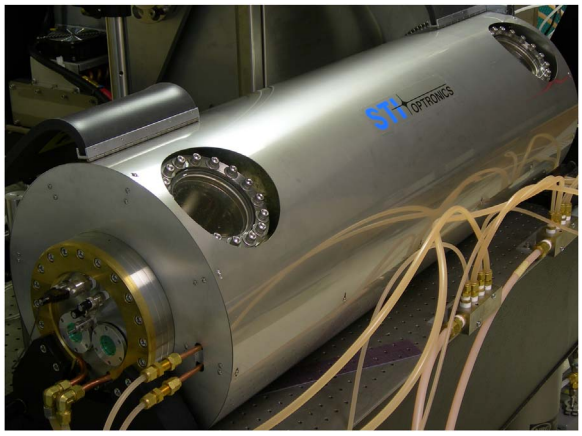

Fig. 9. Photograph of 1-m hot cell. The CO_2 laser beam enters and exits through the windows seen on the end flange. Viewing ports near the ends of the cell are used to facilitate alignment of the laser beam through the cell.

cell. The internal mirror mounts utilize a flexure design and are attached to the end flanges of the cell, which are water-cooled. This ensures the temperature of the mirror mounts stay at ≈150 °C when the CO_2 gas inside the cell is at 400 °C. Custom-made vacuum feedthroughs passing through the end flanges connect to the mirror mounts to permit manually adjusting the mounts. Fig. 9 is a photograph of the hot cell covered with thermal insulation and a stainless-steel jacket.

Alignment of the CO_2 laser beam through the hot cell is done after the cell reaches its operating temperature. This ensures all the components have reached thermal equilibrium and any movements of components caused by thermal expansion have ceased. A HeNe laser beam aligned collinear with the CO_2 laser beam is used for gross alignment. Water-cooled, side-viewing ports are located near each end of the hot cell (see Fig. 9). These ports permit easily viewing the HeNe laser beam being reflected off the internal mirrors. The internal mirrors are flat; therefore, the CO_2 laser beam follows the HeNe laser beam path, thereby, making final alignment of the IR beam through the cell a straightforward process. The same chiller used to cool the MO and the injection-seeded oscillator also cools the hot cell.

Once the hot cell has reached its 400 °C operating temperature at its nominal CO_2 gas pressure of 250 Torr, the mirror mount design has proven to be very robust in maintaining the CO_2 laser beam alignment despite the beam reflecting off five mirrors inside the cell. The alignment of the CO_2 laser beam through the hot cell normally does not need to be readjusted throughout the day.

The truncated laser pulse from the plasma shutter is directed into the hot cell via the left input window seen in Fig. 9. Exiting from the right window is the subnanosecond pulse created by the OFID process. Examples of subnanosecond pulses exiting the cell are shown in Fig. 10 for the *P* and *R* branches. These were obtained using a photovoltaic detector with < 1.5 ns response time. Therefore, the subnanosecond pulse lengths could not be resolved in these oscilloscope traces. Typical energies of these OFID pulses are 20–40 μJ.

An autocorrelator, based upon noncollinear second harmonic generation (SHG) in $AgGaSe_2$, was used to estimate the subnanosecond pulse length emerging from the hot cell. Noncollinear SHG has the advantages of eliminating interference effects and background signal. The optimum phase-matching angle changes with wavelength. Therefore, to accommodate the wavelength range of the laser pulses, the two beams focused into the $AgGaSe_2$ crystal have an angular divergence designed to be within the angular acceptance range of the crystal. This minimized the need for adjustments of the autocorrelator when measuring different wavelengths, but at the price of reduced SHG signal strength. Fortunately, the photovoltaic detector (Vigo Model PV-6) used for detecting the SHG has more than sufficient sensitivity to detect the weaker signals. Scanning of the relative positions of the two pulses inside the $AgGaSe_2$ crystal is performed by manually translating a trombone mirror delay system on the autocorrelator.

Obtaining an estimate of the OFID pulse length requires detecting the SHG signal from multiple shots as the two beams are incrementally translated with respect to each other in the $AgGaSe_2$ crystal. This assumes the pulse length and shape do not change appreciably from shot to shot. Any variations in the length and/or shape will change the SHG signal strength at any given scanning position and, indeed, large fluctuations in the SHG signal were observed leading to significant noise in the autocorrelator data (see Fig. 11). This is a similar noise problem that Kesselring et al. [24] encountered when they measured their OFID pulse lengths using an autocorrelator. Nonetheless, despite the uncertainty in the autocorrelator SHG data, a peak in the SHG signal could be consistently observed at a particular scanning point, which indicated the position of maximum overlap of the two OFID pulses within the $AgGaSe_2$ crystal. As shown in Fig. 11, the width of the peak corresponded to ~100 ps when the hot cell pressure was 200–250 Torr. This is consistent with the results of Kesselring et al. [24], who obtained 35 ps at 500 Torr in their hot cell, and recalling that Mukherjee and Kwok [26] predict an approximate inverse relationship between OFID pulse length and hot cell gas pressure.

We should mention there are other means possible for performing single-shot measurements of subnanosecond IR pulses, such as using a streak camera [5,28]. The BNL-ATF has developed a single-shot autocorrelator that is a variation of the noncollinear SHG scheme [5]. Unfortunately, we did not have access to a streak camera and the BNL-ATF single-shot autocorrelator is designed to measure a few picoseconds, not 100 ps.

3.4. Injection-seeded oscillator

The high-pressure CO_2 laser oscillator is the Model HP3, also manufactured by PAR Systems. It operates at 8.5 bar with a 1:1:14 mixture of $CO_2/N_2/He$. Its maximum pulse repetition rate is 3 Hz. As mentioned, the high pressure helps fill in the gain spectrum and ensures that energy in outlying rotational levels effectively channels energy to the rotational level corresponding to the seed wavelength. The HP3 has its own tuning grating identical in design as the MO except for the turning mirror. The MO turning mirror is flat; whereas, the HP3 turning mirror was custom-made to have a concave radius of curvature of 16.5 m and a 2.5 mm dia. thru-hole located 4.9 mm from the center of the mirror for injection of the seed pulse (see Fig. 4). A flat output coupler (OC) is used on the injection-seeded oscillator, which has different reflectivities depending on the laser line being amplified. The agile tuners on the MO and HP3 are computer-controlled and are set to the same wavelengths. The former selects the wavelength of interest; the latter introduces high cavity losses for all lines except the one of interest.

Fig. 12 shows a typical temporal profile of the output from the injection-seeded oscillator when no seed is injected. It is capable of output pulse energies of 0.5–0.6 J. However, as explained below, due to optical damage problems when amplifying the injection seed, the total pulse energy had to be limited to < 0.3 J.

Table 2 lists the basic specifications for the injection-seeded oscillator.

A small signal gain (SSG) measurement of the injection-seeded oscillator was performed using the MO as the probe beam. A SSG of > 2.4%/cm was measured on the 10P20 line.

Both stable and unstable resonator configurations were tested, where the latter featured a dot mirror on a convex output coupler (−6.0 m radius of curvature). It was found that the unstable resonator was too sensitive to misalignment, and optical damage of the dot mirror was a problem. Therefore, a stable resonator was chosen using a flat OC with its reflective coating facing towards the laser discharge and its opposite side anti-reflection (AR) coated. The AR-coating is

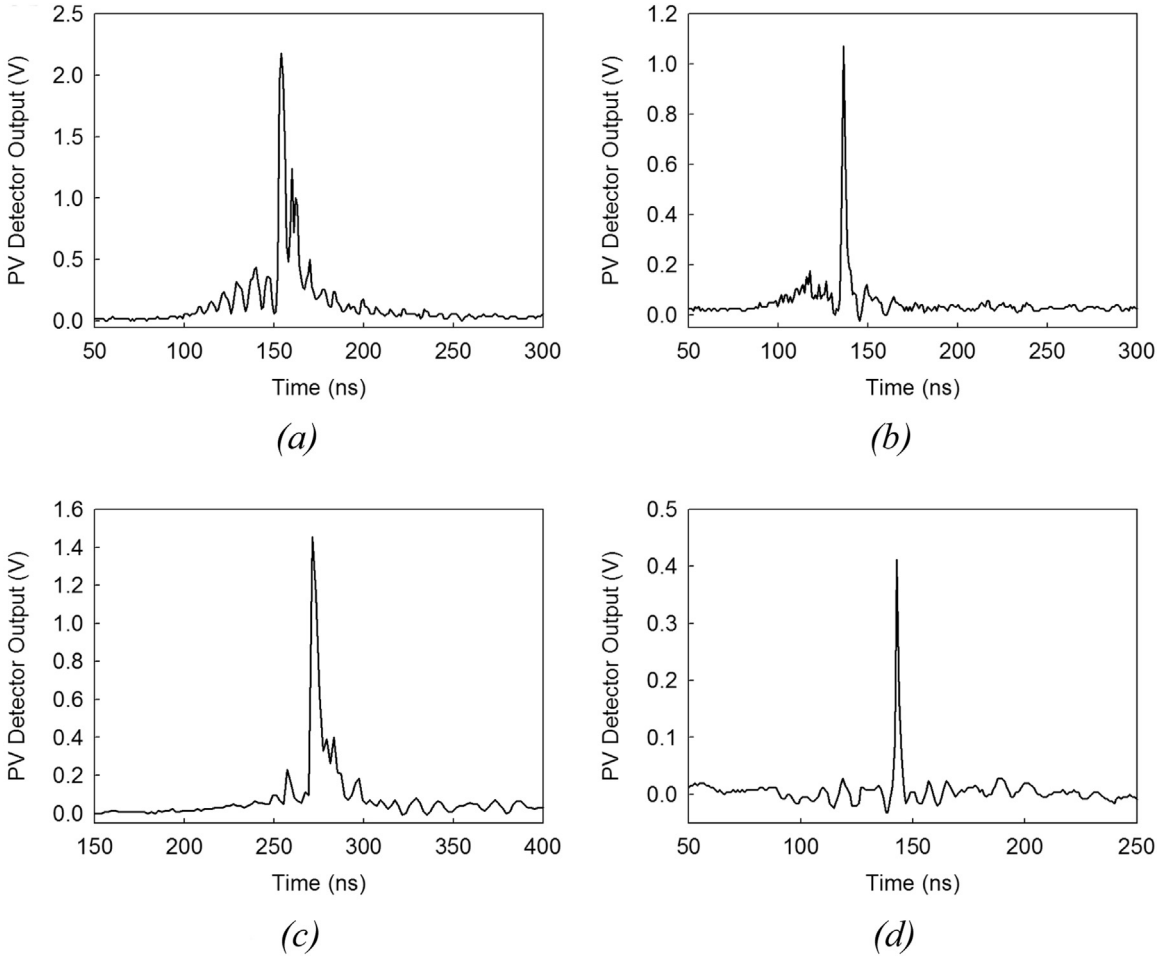

Fig. 10. Examples of ultrashort pulses exiting CO_2 hot cell. (a) 9R8 line. (b) 9P16 line. (c) 10R20 line. (d) 10P16 line.

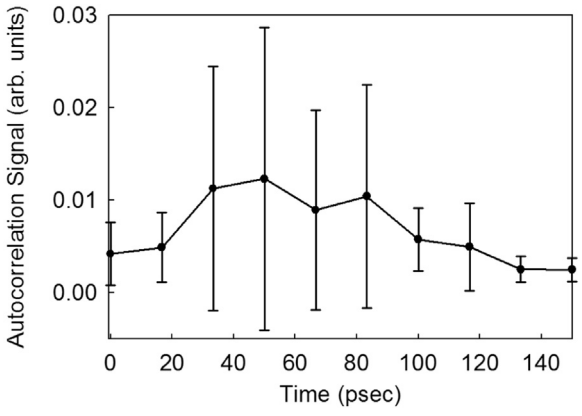

Fig. 11. Example of autocorrelation scan results.

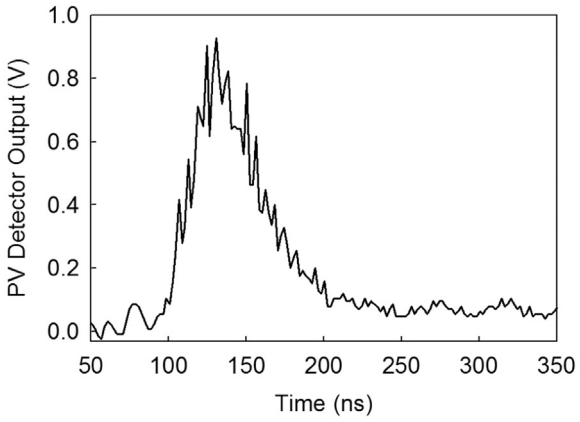

Fig. 12. Typical temporal profile output from injection-seeded oscillator with no injection seed (10P20 line, 315 mJ pulse energy).

important; otherwise significant lasing can occur off the uncoated surface.

As a side note, using an OC with a wedge is not practical because it cannot be easily aligned using a HeNe laser. The wedge causes the HeNe laser beam to refract when it passes through the OC. Therefore, the back reflected HeNe laser spot has no correlation with the transmitted beam. Hence, this OC can only be aligned by sending a HeNe laser beam from the rear of the laser to the output side. Unfortunately, the agile tuner makes it very difficult to send a HeNe laser beam through the rear of the laser.

The HP3 gas chamber uses NaCl windows set at Brewster's angle. The NaCl windows were less susceptible to optical damage than ZnSe windows.

Due to budget limitations, the HP3 did not include a gas regenerator. Instead the HP3 can either operate with a static gas fill, which is typically arc-free for approximately 1800 shots and then the gas must be replaced, or the HP3 can operate by flowing the CO_2 gas mixture through the device at a rate of 50 scfh. The latter permits operating the HP3 for as many shots as the gas in the laser premix bottle provides.

4. Results

Fig. 13 shows typical temporal output beam profiles of the injec-

Table 2
Basic specifications for injection-seeded oscillator.

Parameter	Value
CO_2 gas mixture	1:1:14
Total gas pressure	8.5 bar
Discharge volume	48.6 cm^3
Electrode gap	0.9 cm
Active medium length	60 cm
Maximum repetition rate	3 Hz
Resonator length	125 cm
Output coupler reflectivity	18–70% (depending on laser line)

tion-seeded oscillator when seeded with OFID pulses from the hot cell at representative laser lines within the *P* and *R* branches. We see that trains of subnanosecond pulses are being generated over nearly the entire duration of the oscillator output and the envelope of the trains follows the nominal output pulse shape when the HP3 lases with no injection seeding (c.f. Fig. 12). The pulses within the train are separated by 8.3 ns, which corresponds to the roundtrip time of the 125-cm resonator.

The intracavity fluence inside the injection-seeded oscillator can damage the NaCl windows and/or the AR coating on the OC. This tends to occur when the intracavity fluence exceeds about 1.2 J/cm^2. To reduce the intracavity fluence, a low reflectivity OC must be used, such as 18%R for an uncoated ZnSe OC. However, even with 18%R, the intracavity fluence can still be too high; therefore, the fluence needs to be further reduced by lowering the HP3 high-voltage (HV). The HV can only be lowered a limited amount because the discharge does not reliably breakdown if the voltage is too low. The HP3 nominally operates at a charge voltage of 40–41 kV. The charge voltage can be set as low as 38 kV and still obtain reliable breakdown. This means on the strong laser lines, the OC should not exceed 18%R and the HV should be set to 38 kV. However, it is safe to use higher reflectivity and full HV on the weaker lines and, indeed, as discussed below, this is needed in order to obtain useful injection-seeded output on the weaker lines.

Hot spots can appear on the periphery of the output beam. These can be eliminated by utilizing an intracavity iris to reduce the output beam to 6 mm dia. (Recall the electrode gap spacing of the HP3 is 9 mm).

With these damage-prevention considerations in mind, injection-seeding tests on all the available laser lines from the hot cell were performed where the optimum time for injecting the seed was determined for each individual line. These delay times ranged from 1.8 μs to 4.0 μs before the start of the HP3 lasing output where the stronger lines needed less delay time. Injection-seeding was easily achieved on the strong lines in all the laser bands using the 18%R OC. The less strong lines required a higher OC reflectivity in order to obtain lasing output from the HP3 oscillator. Output couplers with reflectivities of 40%R, 50%R, and 70%R were used. Not surprising, the very weakest lines required the 70%R.

The depth of modulation of the output pulses can be close to 100% as seen in Fig. 13(b)–(d). However, at times only partial modulation is seen, such as in Fig. 13(a) for the 9R8 line, which is a relatively weak line. Indeed, the 9R8 line requires using a 50%R OC and full HV on the HP3. This partial modulation may be due to the broader pedestal at the bottom of the OFID pulse that is observed occasionally in the output from the hot cell [see Fig. 10(a) for the 9R8 line]. The tendency to have

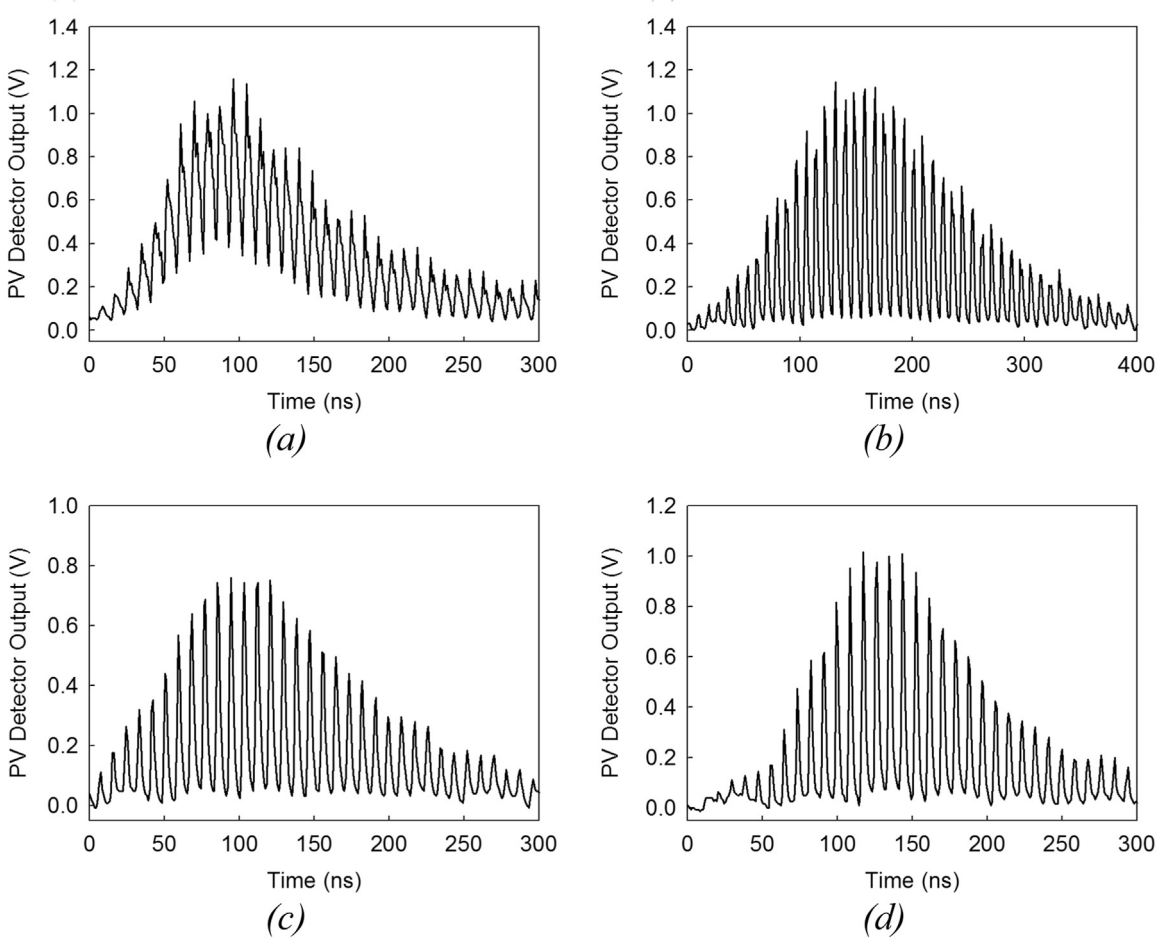

Fig. 13. Examples of amplified pulse trains emitted from injection-seeded oscillator. (a) 9R8 line. (b) 9P16 line. (c) 10R20 line. (d) 10P24 line.

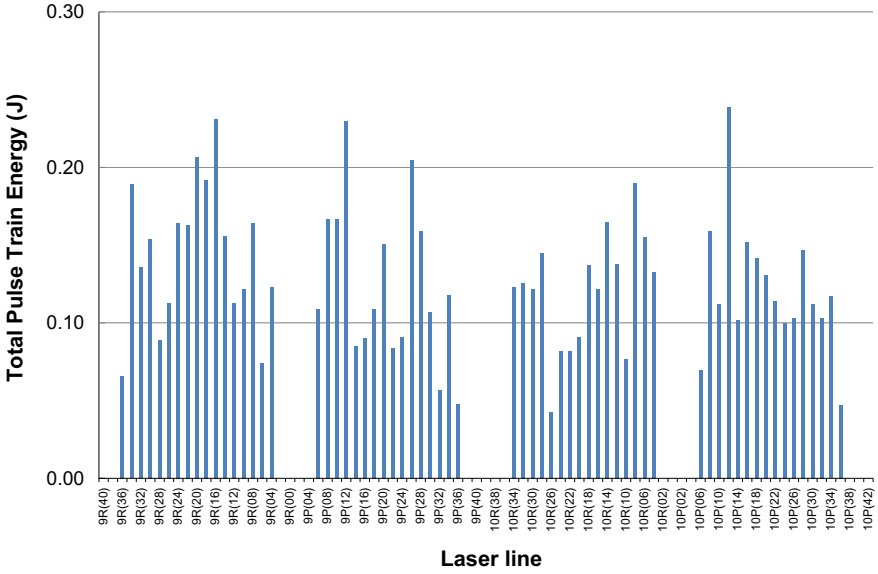

Fig. 14. Total energy in pulse train of injection-seeded oscillator as a function of laser line. Each pulse train has typically 10–20 100-ps pulses.

this broader background underneath the train of ultrashort pulses is more prevalent for the weaker pulses. In other words, the weaker lines often tend to display pulse train profiles similar to Fig. 13(a); whereas, the more well-modulated pulse trains shown in Fig. 13(b)–(d) generally occur with the strong lines. This is discussed more in Section 5.

Successful injection-seeding and pulse train output was demonstrated on nearly all the available MO laser lines, specifically, 9R4 – 9R36, 9P6 – 9P34, 10R4 – 10R34, and 10P6 – 10P36. No lasing output was observed on the 9P36, 9P38, 10R36, 10R38, 10P38, and 10P40 lines. Lasing on these other lines may be possible using an OC with a higher reflectivity, e.g., 95%R, but the amount of output energy may be too small to be useful. Fig. 14 shows the typical total energy in the pulse train for each laser line emitted during injection seeding.

When injection seeding, the total output energy of the HP3 is intentionally limited to less than ~0.3 J in order to avoid damaging the resonator windows. If we assume that the amplified output train of ~100 ps pulses contains roughly 10–20 major pulses, then each of these pulses has a maximum energy of 15–30 mJ corresponding to a peak power of 150–300 MW and a peak flux of 0.76–1.5 GW/cm^2 for a 6-mm dia. output beam.

A look-up table (LUT) was created for setting the various system parameters in order to obtain optimum generation of the subnanosecond pulse train for a particular laser line. Hence, operating the laser system entails the following basic steps. 1) Tune the MO to the desired laser line. 2) From the LUT for the laser line chosen, set the plasma shutter pressure and delay time for triggering the HV spark gap. 3) From the LUT for the laser line chosen, install the specified OC on the HP3 resonator, set the specified HV for driving the HP3, and set the delay time for firing the MO relative to the HP3. 4) Fire all devices from the master delay generator to produce the pulse train. As an aside, in a field-deployed system, it should be possible to automate the changing of the OC reflectivity by, for example, having different OCs mounted on a precision-aligned rotating wheel.

5. Discussion

The maximum pulse energies of the amplified subnanosecond pulses are clearly limited by optical damage. ZnSe windows damaged more easily than the NaCl windows. All windows were uncoated and operated at Brewster's angle. For example, 100-ps pulse energies of 45 mJ corresponding to a total pulse energy of 0.5 J were demonstrated, but at the same time this damaged the NaCl window. At Brewster's angle (56.2°), the laser spot on the NaCl window surface is very elongated; however, damage occurred along the path of the optical beam in the interior of the window.

There is a dearth of data on optical damage thresholds with ultrashort CO_2 laser pulses and essentially none for a train of ultrashort CO_2 laser pulses. For pulse lengths longer than roughly 1 ns, the primary damage mechanism is thermal and has a square-root dependence on the pulse length, e.g., ~1 J/cm^2 at 1 ns and ~10 J/cm^2 at 100 ns for NaCl. For pulse lengths less than 1 ns, the mechanism is dominated by avalanche ionization and the damage threshold becomes independent of pulse length. Thus, we would expect a single 100-ps CO_2 laser pulse to be in this latter regime. However, a train of 100-ps pulses could conceivably alter the damage process. For example, if the time interval between the pulses is less than the free carrier recombination time, then this could make it easier for avalanche ionization to commence in the subsequent pulses; however, with 8.3 ns between pulses, this seems unlikely. Another possibility is that the train of 100-ps pulses effectively creates a ~200 ns pulse (i.e., the pulse width of the train envelope) where thermal damage once again becomes the limiting factor. For a 6-mm diameter beam traversing through our NaCl window, a total pulse energy of 0.3 J, corresponding to 1.1 J/cm^2, did not cause laser damage; whereas, 0.5 J, corresponding to 1.8 J/cm^2 did cause damage. Therefore, it appears the damage mechanism is still primarily due to avalanche ionization. Nevertheless, when damage occurs it tends to be more catastrophic because once one pulse starts to damage the optics, the next pulses in the train cause more damage, thereby resulting in a trail of damage spots seen all along the inside of the NaCl window.

Hence, the system is capable of producing higher pulse energies if a means can be implemented to reduce the fluence on the windows and resonator optics. For example, it may be possible to use intracavity mirrors to expand the resonator mode before it passes through the discharge windows.

The hole in the injection-seeded oscillator for injecting the seed pulse does create a small diffraction effect on the edge of the output beam, which in the near-field is less than 1 mm in size. This diffraction effect does not appear to interfere with the performance of the laser nor contribute to a lower damage threshold. Using a smaller hole and/or moving the hole further away from the cavity axis would reduce this diffraction; however, this was not investigated and it is not known how much this would interfere with effective injection seeding of the oscillator.

Alternative ways for introducing the seed have their drawbacks. Using an intracavity beamsplitter to introduce the seed would eliminate

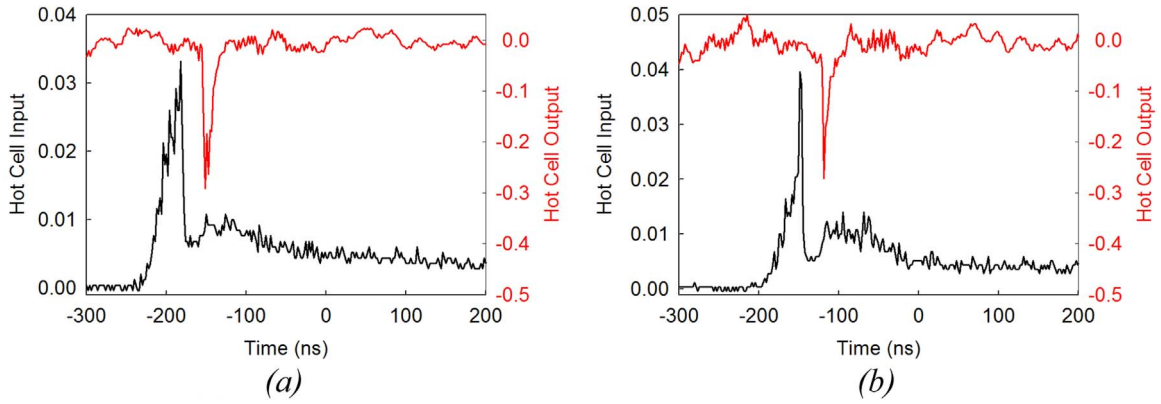

Fig. 15. Comparison of plasma shutter output (black bottom trace) and hot cell output (red top trace) for 10R16 line. (a) Shot 1. (b) Shot 2. (For interpretation of the references to color in this figure legend, the reader is referred to the web version of this article.)

diffraction effects, but it will also lead to considerable cavity losses as the circulating beam reflects off the beamsplitter. Indeed, such a scheme has been used to replace a conventional output coupler, but this also loses the ability to easily vary the output coupling. Injecting the seed through the output coupler at a slight angle relative to the output beam also avoids diffraction effects, but this approach fails when the output coupler reflectivity must be high for the weak laser lines, thereby reflecting away most of the seed pulse energy. Indeed, the seed pulse energy is also weaker on the weak lines, which exacerbates the problem.

The OFID process is straightforward to implement and probably the least expensive way to produce tunable, subnanosecond IR pulses. Nonetheless, it has two limitations. First, the exact pulse length of the OFID pulse appears to vary from shot to shot. Lacking a means for obtaining single-shot measurements of the subnanosecond pulse length, it is not possible to state how much variance occurs. There is indirect evidence that some amount of variance is likely occurring because the shape of the truncated pulse from the plasma shutter tends to vary from shot-to-shot leading to a corresponding change in the OFID pulse seen exiting the hot cell. This is illustrated in Fig. 15, which shows the temporal profiles of the pulse exiting the plasma shutter and the same pulse after exiting the hot cell for the 10R16 line for two different shots. (The pulse exiting the plasma shutter was obtained by detecting back-reflected light from one of the lenses used to collimate the laser light into the hot cell.) The second shot [Fig. 15(b)] has a sharper truncation and it appears the OFID pulse is shorter than the one seen in Fig. 15(a); however, the finite response time of the photovoltaic detector means this is only a qualitative observation.

For the DRRS application, it is less critical that the subnanosecond pulse length be the same from shot-to-shot because its purpose is to excite the molecule of interest. The pulse length can still excite the molecule if the pulse length is, say, a factor of two shorter or longer than 100 ps. However, for other applications, the varying shot-to-shot pulse length could be an issue.

The second limitation is that, as mentioned earlier, the reliability of generating subnanosecond pulse trains from the injection-seeded amplifier varies considerably depending on the strength of the laser line. We believe this is primarily due to the shot-to-shot variance in the output pulse shape from the MO, which affects the truncation occurring in the plasma shutter and, hence, the character of the OFID pulse exiting the hot cell as was noted in Fig. 15. This then affects the depth of modulation of the pulse train because high frequency components, corresponding to the subnanosecond pulse, and lower frequency components, which may be created during the truncation process, are both being injected into and amplified by the injection-seeded oscillator. For example, depending on the exact MO pulse shape, the truncated pulse shape may vary, as illustrated in Fig. 15, and the OFID pulse may have a pedestal. This phenomenon is analogous to the need for high contrast ratio in chirped pulse amplification (CPA) laser systems. The net result is that the depth of modulation of the subnanosecond pulse trains produced by the injection-seeded oscillator tends to vary from shot-to-shot. On the strong laser lines, most of the shots have good depths of modulation. On the weaker lines, just the opposite occurs and few of the shots have good depths of modulation.

For the DRRS application, the temporal profile of the pulse train could be monitored as it is directed at the target gas. Data would be collected when the depths of modulation are within a certain acceptable range. The net impact of this limitation is a reduction in the speed of the data collection process. This can be compensated by increasing the repetition rate of the laser system, in particular, the high-pressure injection-seeded oscillator, which was limited to 3 Hz. Building a high-pressure device that operates at higher repetition rate is certainly feasible. To save on costs for this project, a commercial high-pressure laser was procured, which was only available at 3 Hz. In that regards, for the DRRS application, its sensing range is determined by the laser pulse energy and its speed of detection is affected by the laser average power. With ~30 mJ pulse energy, a sensing range of over 100 m is predicted [6].

6. Conclusions

In conclusion, we have demonstrated for the first time the ability to generate subnanosecond pulse trains over most of the CO_2 laser tuning range with individual pulse energies of up to 30 mJ corresponding to peak powers of 300 MW assuming 100-ps pulse lengths. This laser system would be suitable for remote detection of gaseous agents using a double-resonance technique. In principle, the system could be made sufficiently compact for field deployment. The basic features and characteristics of this system are summarized below.

1) 100-ns seed pulse generated using commercial grating-tuned TEA CO_2 master oscillator.
2) Helium-filled, spark-preionized plasma shutter used to truncate seed pulse.
3) CO_2 hot cell (400 °C) outputs ~100 ps laser pulse via optical free induction decay process.
4) 100-ps pulse used to injection seed commercial, high-pressure, grating-tuned CO_2 oscillator.
5) Injection-seeded oscillator outputs pulse train of 10–20 amplified 100-ps pulses (15–30 mJ) separated by 8.3 ns.
6) Injection-seeding demonstrated over the 9R4 – 9R36, 9P6 – 9P34, 10R4 – 10R34, and 10P6 – 10P36 laser lines.

Acknowledgment

The author wishes to acknowledge S. A. McCormack who designed

and assembled the hot cell, its power supply, and control system. He wishes to thank Dr. H. O. Everitt, Dr. F. C. De Lucia, and D. J. Phillips for their support related to DRRS; Dr. M. N. Polyanskiy for usage of his CO_2 laser code; M. Babzien for advice on the autocorrelator design; and Dr. I. V. Pogorelsky and Dr. C. H. Fisher for their technical advice related to CO_2 lasers. Lastly, he would like to recognize F. Morkel, W. Haarhoff, and G. Louwrens of PAR Systems for their efforts to rectify issues related to the WH10 and HP3 lasers, which were critical for the success of this project. This material is based upon work supported by the Army Contracting Command – Aberdeen Proving Ground, Adelphi, MD under Contract No. W91CRB-11-C-0088.

References

[1] W.D. Kimura, A. van Steenbergen, M. Babzien, I. Ben-Zvi, L.P. Campbell, C.E. Dilley, D.B. Cline, J.C. Gallardo, S.C. Gottschalk, P. He, K.P. Kusche, Y. Liu, R.H. Pantell, I.V. Pogorelsky, D.C. Quimby, J. Skaritka, L.C. Steinhauer, V. Yakimenko, First staging of two laser accelerators, Phys. Rev. Lett. 86 (2001) 4041–4043.

[2] C.A.J. Palmer, N.P. Dover, I. Pogorelsky, M. Babzien, G.I. Dudnikova, M. Ispiriyan, M.N. Polyanskiy, J. Schreiber, P. Shkolnikov, V. Yakimenko, Z. Najmudin, Monoenergetic proton beams accelerated by a radiation pressure driven shock, Phys. Rev. Lett. 106 (1) (2011) 014801.

[3] I.V. Pogorelsky, Ultra-bright x-ray and gamma-source by compton backscattering of CO_2 laser beams, Nucl. Inst. Methods Phys. Res. A 411 (1) (1998) 172–187.

[4] S. Ya. Tochitsky, C. Filip, R. Narang, C.E. Clayton, K.A. Marsh, C. Joshi, Efficient shortening of self-chirped picosecond pulses in a high-power CO_2 amplifier, Opt. Lett. 26 (11) (2001) 813–815.

[5] M.N. Polyanskiy, M. Babzien, I.V. Pogorelsky, Chirped-pulse amplification in a CO_2 laser, Optica 2 (2015) 675–681.

[6] F.C. De Lucia, D.T. Petkie, H.O. Everitt, A double-resonance approach to submillimeter/terahertz remote sensing at atmospheric pressure, IEEE J. Quantum Electron. 45 (2) (2009) 163–170.

[7] P.K. Cheo, Handbook of Molecular Lasers, Marcel Dekker, New York, 1987, pp. 284–289.

[8] J. Xie, Q. Pan, Acousto-optically Q-switched CO_2 laser, in: Laser Systems for Applications, Dr Krzysztof Jakubczak (Ed.), InTech, 2011. http://dx.doi.org/10.5772/25273

[9] N. Hamada, T. Sakai, High-power Q-switched CO_2 laser based on a fast axial gas flow system, in: Proceedings of SPIE 1810, 9th International Symposium on Gas Flow and Chemical Lasers, 53, May 4, 1993. http://dx.doi.org/10.1117/12.144675

[10] P. Lavigne, J. Gilbert, J.L. Lachambre, Passive mode-locking of a large volume TEA-CO_2 laser using an unstable resonator configuration, Opt. Commun. 14 (1975) 194.

[11] A.J. Alcock, A.C. Walker, Generation and detection of 150-psec mode-locked pulses from a multi-atmosphere CO_2 laser, Appl. Phys. Lett. 25 (1974) 299.

[12] A.E. Siegman, Lasers, University Science Books, Mill Valley, 1986, pp. 1104–1116.

[13] A.J. Alcock, P.B. Corkum, Ultra-fast switching of infrared radiation by laser-produced carriers in semiconductors, Can. J. Phys. 57 (1979) 1280.

[14] P.B. Corkum, High-power, subpicosecond 10-μm pulse generation, Opt. Lett. 8 (1983) 514.

[15] I.V. Pogorelsky, et al., Subnanosecond multi-gigawatt CO_2 laser, IEEE J. Quantum Electron. 31 (1995) 556–565.

[16] S. Ya. Tochitsky, R. Narang, C. Filip, C.E. Clayton, K.A. Marsh, C. Joshi, Generation of 160-ps terawatt power CO_2 laser pulses, Opt. Lett. 24 (23) (1999) 1717–1719.

[17] C. Rolland, P.B. Corkum, Generation of 130-fsec midinfrared pulses, J. Opt. Soc. Am. B 3 (12) (1986) 1625–1629.

[18] C.V. Filip, R. Narang, S. Ya. Tochitsky, C.E. Clayton, C. Joshi, Optical Kerr switching technique for the production of a picosecond, multiwavelength CO_2 laser pulse, Appl. Opt. 41 (18) (2002) 3743–3747.

[19] See for example, EKSPLA Models NT370 and PGX01

[20] J. Faist, F. Capasso, D.L. Sivco, C. Sirtori, A.L. Hutchinson, A.Y. Cho, Quantum cascade laser, Science 264 (1994) 553–556.

[21] F. Wang, K. Maussang, S. Moumdji, R. Colombelli, J.R. Freeman, I. Kundu, L. Li, E.H. Linfield, A.G. Davies, J. Mangeney, J. Tignon, S.S. Dhillon, Generating ultrafast pulses of light from quantum cascade lasers, Optica 2 (11) (2015) 944–949.

[22] A.K. Wojcik, P. Malara, R. Blanchard, T.S. Mansuripur, F. Capasso, A. Belyanin, Generation of picosecond pulses and frequency combs in actively mode-locked external ring cavity quantum cascade lasers, Appl. Phys. Lett. 103 (2013) 231102.

[23] R.G. Brewer, R.L. Shoemaker, Optical free induction decay, Phys. Rev. A 6 (1972) 2001.

[24] R. Kesselring, A.W. Kalin, H.J. Schotzau, F.K. Kneubuhl, Picosecond CO_2 laser-pulse generation and amplification, IEEE J. Quantum Electron. 29 (3) (1993) 997–1005.

[25] H.S. Kwok, Eli Yablonovitch, 30-psec CO_2 laser pulses generated by optical free induction decay, Appl. Phys. Lett. 30 (1977) 158–160.

[26] P. Mukherjee, H.S. Kwok, Picosecond time response of a transverse electric atmospheric CO_2 laser amplifier, Appl. Phys. Lett. 44 (1984) 180–181.

[27] D. Haberberger, S. Tochitsky, C. Joshi, Fifteen terawatt picosecond CO_2 laser system, Opt. Express 18 (17) (2010) 17865–17875.

[28] M.N. Polyanskiy, I.V. Pogorelsky, V. Yakimenko, Picosecond pulse amplification in isotopic CO_2 active medium, Opt. Express 19 (8) (2011) 7717–7725.

[29] S. Ya. Tochitsky, J.J. Pigeon, D.J. Haberberger, C. Gong, J. Joshi, Amplification of multi-gigawatt 3 ps pulses in an atmospheric CO_2 laser using ac Stark effect, Opt. Express 20 (2012) 13762–13768.

[30] P.B. Corkum, Amplification of picosecond 10 μm pulses in multiatmosphere CO_2 lasers, IEEE J. Quantum Electron. 21 (1985) 216–232.

[31] M.N. Polyanskiy, co2amp: a software program for modeling the dynamics of ultrashort pulses in optical systems with CO_2 amplifiers, Appl. Opt. 54 (2015) 5136–5142.

[32] P.E. Dyer, D.N. Raouf, Continuously tunable line-narrowed TE CO_2 laser using a near grazing incidence grating, Appl. Opt. 24 (1985) 3152–3154.

[33] H.S. Kwok, E. Yablonovitch, N. Bloembergen, Study of collisionless multiphoton absorption in SF_6 using picosecond CO_2 laser pulses, Phys. Rev. A 23 (1981) 3094–3106.